Improving Object Detection with Inverted Attention

Zeyi Huang Wei Ke Dong Huang *
Carnegie Mellon University
zeyih@andrew.cmu.edu weik@andrew.cmu.edu donghuang@cmu.edu

Abstract

Improving object detectors against occlusion, blur and noise is a critical step to deploy detectors in real applications. Since it is not possible to exhaust all image defects and occlusions through data collection, many researchers seek to generate occluded samples. The generated hard samples are either images or feature maps with coarse patches dropped out in the spatial dimensions. Significant overheads are required in generating hard samples and/or estimating drop-out patches using extra network branches. In this paper, we improve object detectors using a highly efficient and fine-grain mechanism called Inverted Attention (IA). Different from the original detector network that only focuses on the dominant part of objects, the detector network with IA iteratively inverts attention on feature maps which pushes the detector to discover new discriminative clues and puts more attention on complementary object parts, feature channels and even context. Our approach (1) operates along both the spatial and channels dimensions of the feature maps; (2) requires no extra training on hard samples, no extra network parameters for attention estimation, and no testing overheads. Experiments show that our approach consistently improved state-of-the-art detectors on benchmark databases.

1. Introduction

Improving object detectors against image defects such as occlusion, blur and noise is a critical step to deploy detectors in real applications. Recent efforts by computer vision community have collected extensively training data on different scenes, object categories, shapes and appearance. However, it is yet not possible to exhaust all image defects captured under camera shake, dust, fade lighting and tough weather conditions. Moreover, deep learning approaches are highly biased by data distribution, while it is very difficult to collect data with uniform combinations of object features and defects due to the long-tail distribution.

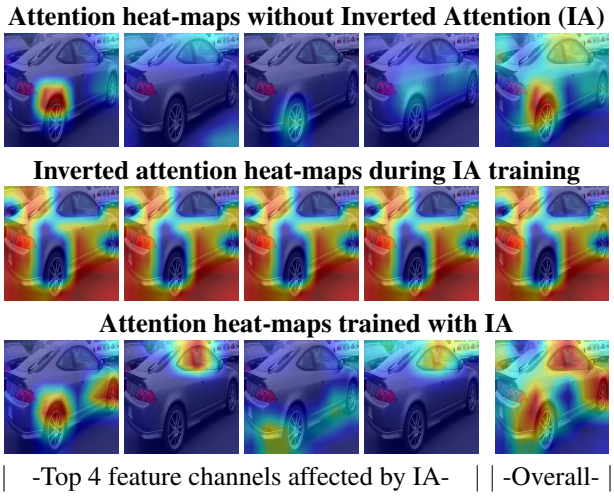

Figure 1: Attention heat-maps visualized at the ROI feature map ($[7 \times 7 \times 512]$) of VGG16 Fast-RCNN. Each $[7 \times 7]$ attention heatmap is linearly interpolated and superposed on the $[224 \times 224]$ object ROI image patch. The first 4 columns are respectively the attention heat-maps at the top 4 channels affected by IA. The last column, "Overall", denotes the overall attention summed over all 512 channels. (This figure is best viewed in color)

Besides waiting for more data collection and annotation, a fundamental way to learn robust detectors is to improve the training approach: (1) Refining models by mining hard samples in training data [17]. These approaches may thoroughly explores the training samples, but does not generalize to defects that are not in training data. (2) Penalizing the occluded bounding boxes by occlusion-aware losses [22, 26]. These approaches do not generalize well to unseen occlusion. (3) Synthesizing image defects by hard example generation [10, 21]. [10] generates new occluded samples by dropping out image patches, and increases the training samples and training cost exponentially. [21] proposes to learn an adversarial network that generates positive samples with occlusions in the feature space. Estimating the occlusion features or masks requires extra networks and therefore

*This work was partially supported by the Intelligence Advanced Research Projects Activity (IARPA) via Department of Interior/ Interior Business Center (DOI/IBC) contract number D17PC00340.

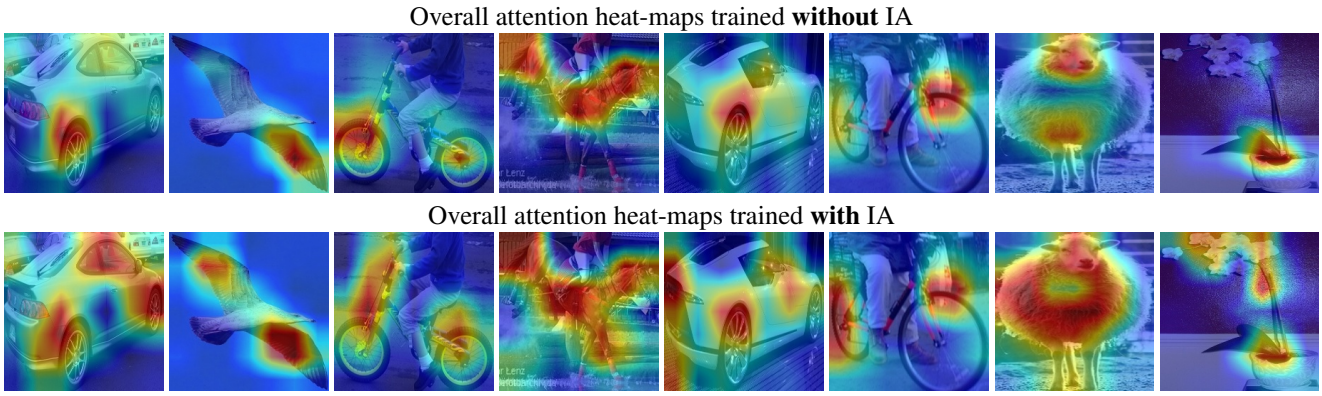

Figure 2: More examples of overall attention heat-maps trained without Inverted Attention (**Upper row**), and trained with Inverted Attention (**Lower row**).

increases the training overheads. In addition, training generator and discriminator simultaneously by competing with each other makes the model hard to converge.

In this paper, we propose Inverted Attention(IA), a simple module added to the standard back-propagation operation. In every training iteration, IA computes the gradient of the feature maps produced at the feature extraction network (also called the backbone network) using object classification scores. The higher gradients on feature maps indicate the more sensitive features. By iteratively invert the gradients at the feature maps, IA re-directs attention of the network to more features. Different from the original detector network that only focuses on the small discriminant parts of objects, the neural network with IA puts more attention on complementary spatial parts of the original network, feature channels and even the context. This is the key that IA can improve the network against unseen defects in inference. In terms of efficiency, the IA module do not have any network parameters to be learned in training. The IA module only changes the network weights in training and does not change any computation in inference.

Fig 1 (the upper row) visualizes the attention in a standard Fast-RCNN detector. The attention is visualized as heatmaps superposed on the object. The red pixels of the heat-maps denote high attention, while the blue pixels denote low attention. During our IA training, the original attention heat-maps are inverted as Fig 1 (the middle row) and proceed to the next iteration. After the IA training finishes, the network produces new attention heat-maps, see Fig 1 (the lower row). Observe that, the detector network trained with IA focuses on more comprehensive features of the objects, making it more robust to the potential defects of the individual pixels. Fig 2 shows more examples of overall attention produced without IA training (the upper row) and with IA training (the lower row).

We summarize the main contributions of this work as follows:

- We propose a highly efficient IA module that fully explore the feature maps along both the spatial and channel dimensions.
- Our IA module requires no extra training on hard samples, no extra network parameters for attention estimation, and no testing overheads.
- We conducts extensive experiments on benchmark datasets where our proposed detector performs favorably against state-of-the-art approaches.

2. Related Work

In this section, we mainly discuss some recent approaches against occlusions and brief introduction about attention mechanism.

2.1. Occlusion-Aware Loss

[26] proposed a aggregation loss for R-CNN based person detectors. This loss enforced proposals of the same object to be close. Instead of using a single RoI pooling layer for a person, the authors used a five-part pooling unit for each person to deal with occlusions. [22] proposed a new bounding box regression loss, termed repulsion loss. This loss encourages the attraction by target, and the repulsion by other surrounding objects. The repulsion term prevents the proposal from shifting to surrounding objects thus leading to more crowd-robust localization. [30] proposed two regression branches to improve pedestrian detection performance. The first branch is used to regress full body regions. The second branch is used to regress visible body regions. Instead of revising network architecture or adding extra loss function to improve occlusion problem, we use a data-driven strategy by generating occluded samples.

2.2. Hard Sample Generation

Image based generation: [28] randomly occludes several rectangular patches of images during training. [10]

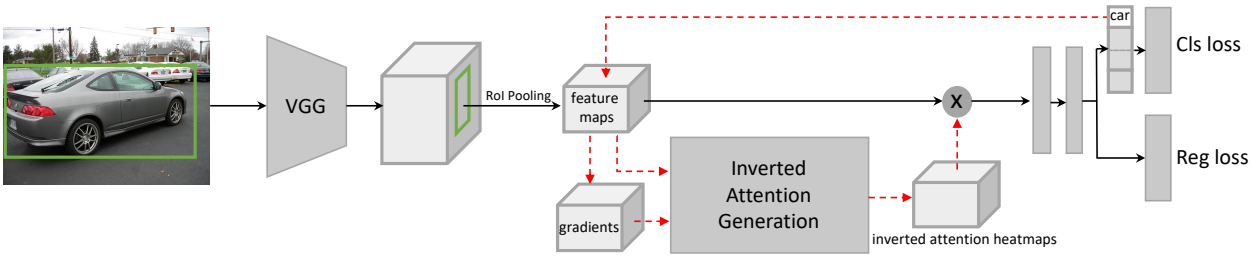

Figure 3: Architecture of Inverted Attention Network (IAN) based on a CNN object detection network. Light gray blocks denote tensors. Dark gray blocks denote operations. The data flows along the red dashed arrows are only needed in training. The inference only require the flows along the black arrows.

occludes rectangular patches of image guided by the loss of the person Re-Identification task. [18] improves weakly-supervised object localization by randomly occluding patches in training images. The hard samples in the image space are often generated in an offline manner, so the training data will increase exponentially.

Feature based generation: [8] selects weighted channel to dropout for the regularization of CNNs. [21] uses predicted occlusion spatial mask to dropout for generating hard positive samples with occlusion and deformations. [27] reweights feature maps according to three kinds of channel-wise attention mechanism. [19] dropout input features to obtain various appearance changes using random generated masks via adversarial learning in video tracking. Unlike existing methods that generate hard samples by adding generative network, we use an efficient IA module which conducts both channel-wise and spatial-wise dropout on features to generate hard samples.

2.3. Attention Estimation

Recent methods incorporate attention mechanism to improve the performance of CNNs. [4, 9, 23] integrate channel-wise or spatial-wise attention network branches to the feed-forward convolutional neural networks. The estimated attention maps are multiplied to the original feature map for various CNN tasks. All these methods introduce extra network branches to estimate the attention maps. [24] improves the performance of a student CNN network by transferring the attention maps of a powerful teacher network. Deconvnet [25] and guided-backpropagation [20] improve gradient-based attention using different backpropagation strategy. CAM [29] converts the linear classification layer into a convolutional layer to produce attention maps for each class. Grad-CAM [16] improve CAM and is applicable to a wide variety of CNN model. In our method, we compute inverted attention guided by gradient-based attention and Grad-CAM. Our network does not require extra network parameters or teacher networks.

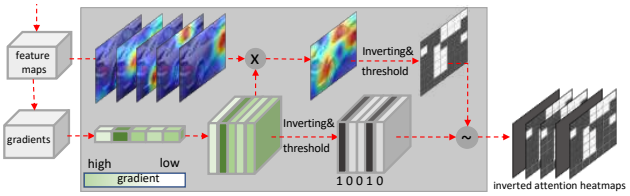

Figure 4: Detailed architecture of the Inverted Attention Generation Module in Fig. 3. This module consists of only simple operations such as pooling, threshold and element-wise product. No extra parameter is needed to learn. This module only operates during training, not in testing.

3. Inverted Attention for Object Detection

We take the R-CNN [5] based framework to illustrate our Inverted Attention Network (IAN) (Fig. 3). An Inverted Attention Generation Module (Fig. 4) is added to the R-CNN detection network, and operates on the ROI featrue maps. Note that this module consists of only few simple operations such as pooling, threshold and element-wise product. No extra parameter is needed to learn. In the rest of the paper, we show how this simple change can effectively improve the original network to overcome image defects.

3.1. Inverted Attention Generation Module

The attention mechanism identifies the most representative receptive field of an object. Highlighting the object with attention heatmaps encourages discrimination between object classes, meanwhile, decreases the diversity of features within the same class. However, the diversity of features is the key to generalize an object detector to unseen object instances and image defects. The proposed Inverted Attention training approach aims to alleviate the conflict and find the optimal trade-off between discrimination and diversity.

As shown in Fig. 4, the Inverted Attention Generation Module consists of two simple operations: (1) Gradient-Guided Attention Generation: computing the the gradients at feature maps, by back propagating only the classification

(a) Epoch 1 (b) Epoch 2 (c) Epoch 3 (d) Epoch 4 (e) Epoch 5 (f) Epoch 6 (g) Epoch 7 (h) Epoch 8

Figure 5: Network attention evolves at different epochs during the IA training. Each sub-image shows the 2D attention heat-maps superposed on object ROI. The attention maps are visualized at the ROI feature map ($[7 \times 7 \times 512]$) of the VGG16 backbone network in Fast-RCNN.

score on the ground-truth category, (2) Attention Inversion: reversing element values of the attention tensor to produce IA heat-maps.

Gradient-Guided Attention Generation: In training phase of the convolutional neural networks, gradients of feature maps in the back-propagation operation encode how sensitive the output prediction is with respect to changes at the same location of the feature maps. If small changes at an element of feature maps have a strong effect on the network outputs, then the network will be updated to pay more attention on that feature element. With this principle, we use the gradient to generate attention map in our approach (see details in Fig.4).

Denote the gradient tensor as $\mathbf{G}$[1] and feature tensor as $\mathbf{F}$. Both of them are of size $height \times width \times channel$. A global pooling is applied on the gradient tensor to produce a weight vector $\mathbf{w}$ with size $channel \times 1$. We compute a gradient guided attention map following [16],

$$\mathbf{M} = \sum_{i}^{channel} w_i * \mathbf{F}^{(i)}, \tag{1}$$

where w_i is the i-th element of $\mathbf{w}$, and $\mathbf{F}^{(i)}$ is the i-th channel map of $\mathbf{F}$. As shown in Fig. 4, the high values in gradient correspond to the receptive field of and trunk in the car sample, while small values correspond to the receptive field of door of the car and background.

Attention Inversion: In the standard training process, the gradient descent algorithm forces the attention map to converge to a few most sensitive parts of objects, while ignoring the other less sensitive parts of objects. The IA training conducts iterative inverting of the original attention tensor as the *Inverted Attention* tensor, which forces the network to detect object based on their less sensitive parts. Specifically, we generate a spatial-wise inverted attention map and a channel-wise inverted attention vector, and then combine them to produce the final attention maps.

The spatial-wise inverted attention map $\mathbf{A}^s = \{a_i^s\}$ is computed as

$$a_i^s = \begin{cases} 0 & \text{if } m_i > T_s \\ 1 & \text{else} \end{cases}, \tag{2}$$

where a_i^s and m_i are the elements of $\mathbf{A}^s$ and $\mathbf{M}$ at the i-th pixel, respectively. T_s is the threshold for spatial-wise attention map. From Eq. 2, spatial-wise inverted attention map pays more attention to the area of the sample with small gradient value.

Observe that the weight vector $\mathbf{w}$ serves as a sensitivity measure for channels of feature maps. A threshold T_c is used to compute the channel-wise inverted attention vector $\mathbf{A}^c = \{a_j^c\}$,

$$a_j^c = \begin{cases} 0 & \text{if } w_j > T_c \\ 1 & \text{else} \end{cases}. \tag{3}$$

The final inverted attention map $\mathbf{A} = \{a_{i,j}\}$ is computed as

$$a_{i,j} = \begin{cases} a_i^s & \text{if } a_j^c = 0 \\ 1 & \text{else} \end{cases}. \tag{4}$$

Fig. 5 illustrates how network attention evolves at different epochs during the IA training. The IA training iteratively guides the neural network to extract features on the whole object sample.

3.2. Inverted Attention Network

As shown in Fig. 3, the Inverted Attention Network (IAN) is basically built by adding Inverted Attention Generation Module (Fig. 4) to the R-CNN based detection network, and operates on the ROI feature maps.

[1]All non-bold letters represent scalars. Bold capital letter $\mathbf{X}$ denotes a matrix; Bold lower-case letters $\mathbf{x}$ is a column vector. $\mathbf{x_i}$ represents the i^{th} column vector of the matrix $\mathbf{X}$. x_j denotes the j^{th} element of $\mathbf{x}$.

Given an input image, the backbone of the R-CNN framework, *i.e.*, VGG or ResNet, takes the whole image as an input and produces feature maps. The region proposals are generated from these feature maps by region proposal network (RPN) or pre-computed region proposal candidates. Then the RoI-pooling layer generates a fixed size feature maps for each object proposal. These feature maps after RoI pooling then go through fully connected layers for object classification and bounding box regression.

The R-CNN can be trained end-to-end by optimizing the following two loss functions:

$$L_{rpn} = L_{cross-entropy} + L_{rpn\_reg}, \tag{5}$$

$$L_{rcnn} = L_{softmax} + L_{rcnn\_reg}, \tag{6}$$

where $L_{cross-entropy}$ and L_{rpn_reg} are the cross-entropy loss and L1 loss for RPN network. $L_{cross-entropy}$ and L_{rpn_reg} are the softmax loss and L1 loss for RCNN network. $L_{rpn} + L_{rcnn}$ are jointly optimized in the Faster-RCNN framework, and L_{rcnn} is optimized in the Fast-RCNN framework.

In the backward stage, the gradient is computed by back-propagating the classification score only on the ground-truth category, which is used for inverted attention generation module. With the generated Inverted Attention map, an element-wise product layer between feature maps and IA heat-maps is used for feature refinement, as

$$\mathbf{F_{new}} = \mathbf{F}. * \mathbf{A}, \tag{7}$$

where $.*$ indicates element-wise multiplication. The refinement is conducted at element-level, i.e., along both the spatial and channels dimensions of the feature maps.

After these operations, the refined features are forwarded to compute the detection loss, and then the loss is back-propagated to update the original network parameters. The training process of IAN is summarized in Algorithm 1.

3.3. Discussion

The high attention regions learned by the original network represent the most common features shared by the training samples. These features are discriminative enough on the training data while may not be enough for the testing data, especially when high attention regions are corrupted by the unseen image defects.

Most top improvements on original networks were reached by discovering more discriminative features. For instance, Image based Hide-and-Seek (HaS) [28] and feature based A-Fast-RCNN [21]. HaS randomly hides patches in a training image, forcing the network to seek discriminative features on remaining patches of the images. A-Fast-RCNN finds the best patches to occlude by estimating a occlusion mask with a generation and adversary network.

Algorithm 1 Training Process of IAN

Input: RGB images with ground-truth labels
Output: Object detection model.

1: **for** each iteration **do**
2: Generating region proposal by the RPN network;
3: Getting the the feature map of the region proposal by ROI pooling, as F shown in Fig. 3;
4: Computing gradient G by back propagating the classification score on the ground-truth category;
5: Computing the gradient-guided attention map with Eq. 1;
6: Achieving spatial-wise and channel-wise inverted attention maps with Eq. 2 and Eq. 3;
7: Refining feature map F with inverted attention map with Eq. 7;
8: Computing RPN loss and classification loss with Eq. 5 and Eq. 6;
9: Back-propagation.
10: **end for**

Our IA approach fuses the advantages of both approaches in the training steps of the original detector network. The new discriminative features are iteratively discovered (see Fig. 5) by inverting the original attention. IA finds discriminative features in all object parts, feature channels and even context. This process requires no extra training epochs on hard samples and no extra network parameters to estimate occlusion mask.

4. Experiments

Inverted Attention Network (IAN) was evaluated on three widely used benchmarks: the PASCAL VOC2007, PASCAL VOC2012 [3], and MS-COCO [12] datasets. In the following section, we first introduce the experimental settings, then analyze the effect of the Inverted Attention module. Finally, we report the performance of IAN and compare it with the state-of-the-art approaches.

We used Faster-RCNN and Fast-RCNN object detctors as our baselines. Our IANs are simply constructed by adding the IA module to each baseline network. VGG16 and ResNet-101 were used as the backbone feature extractors. By default, Fast R-CNN with VGG16 were used in ablation study. The standard Mean Average Precision (mAP) [3] are used as the evaluation metric. For PASCAL VOC, we report mAP scores using IoU thresholds at 0.5. For the COCO database, we use the standard COCO AP metrics.

4.1. Experimental Settings

4.1.1 Implementation Details

PASCAL VOC2007: All models were trained on the VOC2007 trainval set and the VOC2012 trainval set, and

tested on the VOC2007 test set. For Fast-RCNN, we followed the training strategies in [21]: set the learn rate to $2e^{-3}$ for the first 6 epochs, and decay it to $2e^{-4}$ for another 2 epochs. We used batch size 2 in training, and used VGG16 as the backbone networks for all the ablation study experiments on the PASCAL VOC dataset. For Faster-RCNN, we followed the training strategies in [15]: set the learn rate to $2e^{-3}$ for the first 6 epochs, and decay it to $2e^{-4}$ for another 2 epochs. We used the batch size 2 in training. We also report the results of ResNet101 backbone on these models.

PASCAL VOC2012: All models were trained on the VOC2007 trainval set, VOC2012 trainval set and VOC2007 test set, and then tested on the VOC2012 test set. For Faster-RCNN experiments, we follow the exact same training strategies as the VOC2007 training above.

COCO: Following the standard COCO protocol, training and evaluation were performed on the $120k$ images in the trainval set and the $20k$ images in the test-dev set respectively. For Faster-RCNN, we set the learn rate to $1e^{-2}$ for the first 8 epochs, decay it to $1e^{-3}$ for another 3 epochs and $1e^{-4}$ for the last 1 epochs. We used batch size 16 in training, and used ResNet101, ResNetXt-101, ResNet50-FPN, and ResNet101-FPN as the backbone networks.

4.1.2 Parameter Settings

IA only has two parameters: the spatial-wise threshold T_s and the channel-wise threshold T_c (in Eq. 2 and Eq. 3). We take soft-threshold strategy, which is compared with other threshold selection in detail in Sec. 4.3.1. For spatial-wise inverted attention map $height \times width$, we set the gradients of 33% feature elements that have highest values to zero. For channel-wise inverted attention map, we dropout top 80% pixels with highest values.

In order to prevent network from overfitting to the inverted feature maps, we only apply IA on 20% region proposals' feature maps, and leave the rest 80% region proposals' feature maps unchanged.

4.2. Training Speed

The forward cost increases a little due to IA operations such as pooling, threshold and element-wise product. The backward cost increases a little due to backpropagating head parts of the detector network. Training time comparison between Faster-RCNN and our method is shown in Table 1.

4.3. Results on PASCAL VOC2007

To verify the effectiveness of Inverted Attention, we first conducted ablation study on two key factors of IA, *i.e.*, inversion strategies and inversion orientation. By taking the best settings in the ablation study, we then show the results compared with baselines and state-of-the-art.

Method	Backbone	Batch Size	Time (hours/epoch)
Faster-RCNN	VGG	16	0.19
Faster-RCNN + IA (ours)	VGG	16	0.20
Faster-RCNN	Resnet101	16	6.0
Faster-RCNN + IA (ours)	Resnet101	16	6.5

Table 1: Training time comparison between Faster-RCNN and our method on single Titian XP.

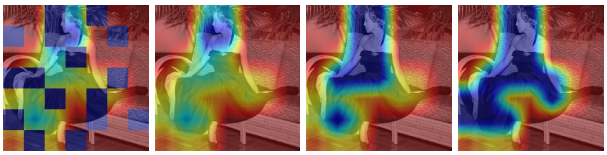

(a) (b) (c) (d)

Figure 6: Visualization of four inversion strategies. From (a) to (d), it illustrates inverted attention map by random, overturn, hard-threshold, and soft-threshold, respectively.

Method	mAP
Baseline (Fast-RCNN + VGG16)	69.1
Random	70.3
Overturn	70.6
Hard-threshold	70.9
Soft-threshold	**71.4**

Table 2: Ablation study on inversion strategies.

Method	mAP
Spatial	71.4
Channel	70.9
Spatial + Channel	**71.6**

Table 3: Ablation study on inverted orientations.

4.3.1 Ablation Study

The following ablation study is conducted on the Fast-RCNN with the VGG16 backbone.

Inversion Strategies: Four inversion strategies were evaluated: Random inversion, Overturn inversion, Hard-threshold inversion, and Soft-threshold inversion. Table 2 shows that all the four inverting strategies improve the performance of the baseline. Fig. 6 visualize the four strategies on the same on the same object.

As shown in Fig. 6a, by randomly selecting pixels on convolutional feature maps and setting them to 0, the mAP improves from 69.1% to 70.3%. However, random inversion loses the contextual information, meaning that even in the same semantic part, some pixels were kept while others were discarded. As shown in Fig. 6b Overturn inversion achieves inverted attention map by IA = 1.0 - A, which increases the weight of background and suppresses

Method	Train	Backbone	mAP	aero	bike	bird	boat	bottle	bus	car	cat	chair	cow	table	dog	horse	bike	person	plant	sheep	sofa	train	TV
FRCN [5]	07	VGG16	69.1	**75.4**	80.8	67.3	59.9	37.6	**81.9**	80.0	84.5	50.0	77.1	68.2	81.0	82.5	74.3	69.9	28.4	71.1	70.2	75.8	66.6
Fast+ASTN [21]	07	VGG16	71.0	74.4	81.3	67.6	57.0	46.6	81.0	79.3	**86.0**	**52.9**	75.9	**73.7**	**82.6**	83.2	**77.7**	72.7	37.4	66.3	**71.2**	78.2	74.3
Fast+IA(ours)	07	VGG16	**71.6**	74.9	**82.0**	**71.8**	59.1	**47.6**	80.9	**80.5**	85.2	51.2	**77.2**	71.6	81.3	83.6	77.0	**74.1**	39.3	**71.1**	70.0	**79.2**	74.0
FRCN [5]	07	ResNet101	71.8	**78.7**	82.2	71.8	55.1	41.7	79.5	80.8	88.5	53.4	81.8	72.1	87.6	85.2	80.0	72.0	35.5	71.6	75.8	**78.3**	64.3
Fast+ASTN [21]	07	ResNet101	73.6	75.4	**83.8**	75.1	61.3	44.8	**81.9**	**81.1**	87.9	57.9	81.2	**72.5**	87.6	**85.2**	80.3	74.7	**44.3**	72.2	76.7	76.9	71.4
Fast+IA(ours)	07	ResNet101	**74.7**	77.3	81.2	**78.1**	**62.6**	**52.5**	77.8	80.0	**88.7**	**58.6**	**81.8**	71.4	**87.9**	84.2	**81.4**	**76.6**	44.0	**77.1**	**79.1**	76.9	**77.2**
Faster [15]	07	VGG16	69.9	70.0	**80.6**	**70.1**	**57.3**	49.9	78.2	80.4	82.0	**52.2**	75.3	**67.2**	80.3	79.8	75.0	76.3	39.1	68.3	67.3	**81.1**	67.6
Faster+IA(ours)	07	VGG16	**71.1**	**73.4**	78.5	68.3	54.7	**56.1**	**81.0**	**85.5**	**84.3**	48.4	**77.9**	61.7	**80.5**	**82.6**	**75.3**	**77.5**	**47.0**	**71.7**	**68.8**	76.0	**72.5**
Faster [15]	07	ResNet101	75.1	76.5	79.7	77.7	66.4	61.0	83.3	86.3	**87.5**	53.6	81.1	66.9	85.3	**85.1**	77.4	**78.9**	**50.0**	74.1	**75.8**	78.9	75.4
Faster+IA(ours)	07	ResNet101	**76.5**	**77.9**	**82.9**	**78.4**	**67.2**	**62.2**	**84.2**	**86.9**	87.2	**55.5**	**85.6**	**69.1**	**87.0**	85.0	**81.4**	78.8	48.4	**79.4**	75.0	**83.2**	**75.4**
Faster [15]	07+12	VGG16	73.2	76.5	79.0	70.9	65.5	52.1	83.1	84.7	86.4	52.0	**81.9**	65.7	84.8	84.6	77.5	76.7	38.8	73.6	73.9	83.0	72.6
Faster+IA(ours)	07+12	VGG16	**76.8**	**78.5**	**81.1**	**76.8**	**67.2**	**63.9**	**87.1**	**87.7**	**87.8**	**59.3**	81.1	**72.9**	**84.8**	**86.7**	**80.5**	**78.7**	**50.9**	**76.9**	**74.2**	**83.1**	**76.5**
Faster [15]	07+12	ResNet101	76.4	79.8	80.7	76.2	68.3	55.9	85.1	85.3	**89.8**	56.7	**87.8**	69.4	**88.3**	**88.9**	80.9	78.4	41.7	78.6	79.8	85.3	72.0
Faster+IA(ours)	07+12	ResNet101	**81.1**	**85.3**	**86.8**	**79.7**	**74.6**	**69.4**	**88.4**	**88.7**	88.8	**64.8**	87.3	**74.7**	87.7	88.6	**85.3**	**83.5**	**53.9**	**82.7**	**81.5**	**87.8**	**80.9**

Table 4: Object detection Average Precision (AP) tested on VOC2007. We followed the same training prototype as the baselines without adding any extra tricks or data augmentations.

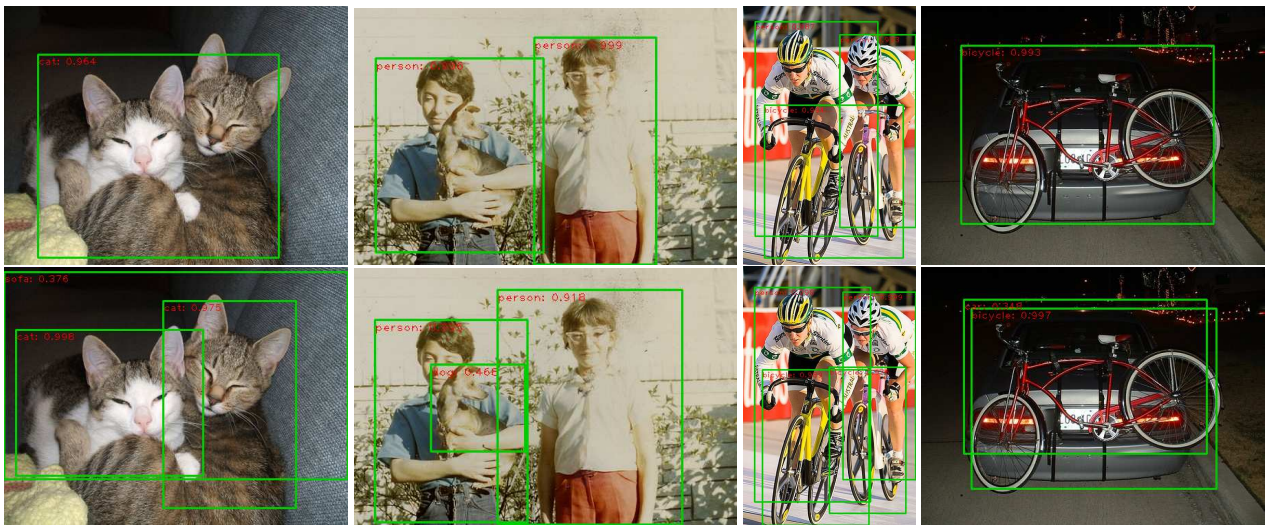

Figure 7: Object detection examples in VOC2007 with ResNet101-Faster-RCNN (top) and its IAN version (bottom).

the foreground. Overturn inversion gets the mAP of 70.6%, which is 1.5 percentages better than baseline. To keeping the weights of background, we take two thresholding methods to suppresses all pixels in attention map which are large than the threshold. The hard-threshold is shown in Fig. 6c, which takes 0.5 as threshold. While the soft-threshold adopts a sorting algorithm and suppresses the top 33% pixels. Hard-threshold achieves 70.9% mAP and soft-threshold achieves 71.4%, which are 1.8% and 2.3% better than the baseline, respectively.

Inversion Orientation: Using the soft-threshold inversion strategy, we further studied two inversion orientations in Table 3. The spatial inversion attention conducts inversion over all channels, while the channel inversion attention conducts inversion only on a subset of channels. Conducting spatial or channel inversion produced 71.4% and 70.9%, respectively. Conducting both the spatial and channel inversion, the performance is further improved to 71.6%.

4.3.2 Comparing with Baselines and State-of-the-Art

We first present extensive comparisons on PASCAL VOC 2007 with Fast-RCNN (denoted as "FRCN"), Faster-RCNN (denoted as "Faster") and the state-of-the-art hard-sample generation approaches Fast-RCNN with ASTN [21] (denoted as "Fast+ASTN"). These approaches only provided results on Fast-RCNN. The results are compared in Table 4.

With the VGG16 backbone and the VOC2007 training data, IA improved Fast-RCNN from 69.1% to 71.6%, and improves Faster-RCNN form 69.9% to 71.1%, which are 2.5% and 1.2% improvement respectively. With more powerful backbone, *i.e.*, ResNet101, Fast-RCNN and Faster-RCNN achieves better object detection performance than VGG16. By adding IA to them, the performance were consistently improved: for Fast-RCNN from 71.8% to 71.4%, and for Faster-RCNN from 75.1% to 76.5%, respectively. Using the training data from both VOC2007 and VOC2012,

Method	Train	Backbone	mAP	aero	bike	bird	boat	bottle	bus	car	cat	chair	cow	table	dog	horse	bike	person	plant	sheep	sofa	train	TV
Faster [15]	07++12	ResNet101	73.8	86.5	81.6	77.2	58.0	51.0	78.6	76.6	93.2	48.6	80.4	59.0	**92.1**	85.3	84.8	80.7	48.1	77.3	66.5	84.7	65.6
Faster+IA(ours)	07++12	ResNet101	**79.2**	**87.7**	**86.7**	**80.3**	**68.1**	**62.1**	**81.0**	**84.7**	**93.8**	**61.8**	**84.2**	**63.1**	92.0	**87.4**	**86.6**	**85.8**	**61.0**	**84.6**	**72.4**	**86.5**	**73.8**

Table 5: Object detection Average Precision (AP) tested on PASCAL VOC2012. We followed the same training prototype as the baselines without adding any extra tricks or data augmentations.

Method	Backbone	Schedule	$AP_{[0.5,0.95]}$	$AP_{0.5}$	$AP_{0.75}$	AP_s	AP_m	AP_l
YOLOv2 [14]	DarkNet-19	-	21.6	44.0	19.2	5.0	22.4	35.5
SSD512 [13]	ResNet101	-	31.2	50.4	33.3	10.2	34.5	49.8
RetinaNet [11]	ResNet101-FPN	-	39.1	59.1	42.3	21.8	42.7	50.2
Faster-RCNN [15]	ResNet101-FPN	-	36.2	59.1	39.0	18.2	39.0	48.2
Deformable R-FCN [2]	Inception-ResNet-v2	-	37.5	58.0	40.8	19.4	40.1	52.5
Mask-RCNN [7]	ResNet101-FPN	-	38.2	60.3	41.7	20.1	41.1	50.2
Faster-RCNN* [1]	ResNet50-FPN	1x	36.2	58.5	38.9	21.0	38.9	45.3
Faster-RCNN* [1]	ResNet101-FPN	1x	38.8	60.9	42.1	22.6	42.4	48.5
Faster-RCNN* [1]	ResNet101-FPN	2x	39.7	61.3	43.4	22.1	43.1	50.3
Faster-RCNN* [1]	ResNetXt101-32x4d-FPN	1x	40.5	62.7	43.9	24.1	43.9	50.3
Faster-RCNN* [1]	ResNetXt101-64x4d-FPN	1x	41.6	64.0	45.4	24.9	45.2	52.1
Mask-RCNN* [1]	ResNet101-FPN	1x	39.7	61.6	43.2	23.0	43.2	49.7
Faster-RCNN*+IA(ours)	ResNet50-FPN	1x	**38.3**(+2.1)	59.7(+1.4)	41.8(+1.9)	21.9(+0.9)	41.0(+1.1)	47.6(+2.3)
Faster-RCNN*+IA(ours)	ResNet101-FPN	1x	**40.2**(+1.4)	61.6(+0.7)	44.1(+2.0)	22.9(+0.3)	43.1(+0.7)	50.7(+2.2)
Faster-RCNN*+IA(ours)	ResNet101-FPN	2x	**40.8**(+1.1)	61.9(+0.6)	44.8(+1.4)	22.6(+0.5)	43.7(+0.6)	51.9(+1.6)
Faster-RCNN*+IA(ours)	ResNetXt101-32x4d-FPN	1x	**41.7**(+1.2)	63.3(+0.6)	45.8(+1.9)	24.8(+0.7)	44.7(+0.8)	52.3(+2.0)
Faster-RCNN*+IA(ours)	ResNetXt101-64x4d-FPN	1x	**42.8**(+1.2)	63.8(-0.2)	47.2(+1.8)	25.3(+0.4)	45.8(+0.6)	53.6(+1.5)
Mask-RCNN*+IA(ours)	ResNet101-FPN	1x	**41.0**(+1.3)	62.0(+0.4)	45.1(+1.9)	23.6(+0.6)	43.8(+0.6)	52.0(+2.3)

Table 6: Comparing with state-of-the-art methods on COCO test-dev (single scale testing). The numbers in brackets are performance gains of IA. The symbol * denotes the latest re-implemented results from [1] (typically better than the original papers). Training "Schedule"s used here were introduced in Detectron [6].

the mAPs of our approach were further improved to 76.8% with VGG16, and 81.1% with ResNet101.

Fig. 7 shows some detection examples from the VOC2007 test set using ResNet101 Faster-RCNN and its IAN version. These examples illustrate that IAN improves object detection to handle images defects such as heavy occlusions, faded pictures and shadows.

4.4. Results on PASCAL VOC2012 and COCO2017

We implemented IA based on Faster-RCNN and Mask-RCNN respectively. For the PASCAL VOC2012 and COCO2017 datasets, all results were produced by the official evaluation server.

The performance on PASCAL VOC2012 is shown in Table 5. For ResNet101 Faster-RCNN, IA increased mAP from 73.8 of the baseline to 79.2, which is 5.4 improvement. The AP on 19 categories achieved consistent performance gain. This demonstrates that our IAN can discover more discriminative features for a large variety of object classes.

The detection performance of COCO2017 is shown in Table 6. We used the official evaluation metrics for COCO. We used a better implementation [1] as our strong baseline. IA gets 2.1 higher AP with ResNet50-FPN and achieves 38.3 AP without bells and whistles. When using more powerful backbone ResNetXt101-64x4d or longer training schedule on ResNet101-FPN, IA gains over 1.0 AP than baselines consistently. IA also gain 1.3 higher AP for bounding box evaluation in Mask-RCNN [7] framework.

The COCO evaluation server also gave the detection performance on small (AP_s), medium(AP_m), and large objects(AP_l). It is interesting to note that, in Table 6, IAN tends to boost the performance of the large objects than the small objects. This indicates that larger objects have more features discovered by IAN. One can also observe that IA tends to boost the localization accuracy as the AP of IoU=0.75 gains more than AP of IoU=0.50. The higher detection IoU means that the detector finds more features of each object for localization purposes, rather than settle with few discriminative parts of objects. This further validates the discussion in Sec. 3.3 and examples in Fig. 5.

5. Conclusion

We present IA as a highly efficient training module to improve the object detection networks. IA computes attention using gradients of feature maps during training, and iteratively inverts attention along both spatial and channel dimension of the feature maps. The object detection network trained with IA spreads its attention to the whole objects. As a result, IA effectively improves diversity of features in training, and makes the network robust to image defects. It is very attractive to explore the best configurations of IA module on all other computer vision tasks such as image classification, instance segmentation and tracking.

References

[1] K. Chen, J. Wang, J. Pang, Y. Cao, Y. Xiong, X. Li, S. Sun, W. Feng, Z. Liu, J. Xu, et al. Mmdetection: Open mmlab detection toolbox and benchmark. *arXiv preprint arXiv:1906.07155*, 2019. 8

[2] J. Dai, Y. Li, K. He, and J. Sun. R-fcn: Object detection via region-based fully convolutional networks. In *Advances in neural information processing systems*, pages 379–387, 2016. 8

[3] M. Everingham, L. J. V. Gool, C. K. I. Williams, J. M. Winn, and A. Zisserman. The pascal visual object classes (VOC) challenge. *International Journal of Computer Vision*, 88(2):303–338, 2010. 5

[4] J. Fu, J. Liu, H. Tian, Z. Fang, and H. Lu. Dual attention network for scene segmentation. *arXiv preprint arXiv:1809.02983*, 2018. 3

[5] R. Girshick. Fast r-cnn. In *Proceedings of the IEEE international conference on computer vision*, pages 1440–1448, 2015. 3, 7

[6] R. Girshick, I. Radosavovic, G. Gkioxari, P. Dollár, and K. He. Detectron. https://github.com/facebookresearch/detectron, 2018. 8

[7] K. He, G. Gkioxari, P. Dollár, and R. Girshick. Mask r-cnn. In *Proceedings of the IEEE international conference on computer vision*, pages 2961–2969, 2017. 8

[8] S. Hou and Z. Wang. Weighted channel dropoutfor regularization of deep convolutional neural network. In *AAAI*, 2019. 3

[9] J. Hu, L. Shen, and G. Sun. Squeeze-and-excitation networks. In *Proceedings of the IEEE conference on computer vision and pattern recognition*, pages 7132–7141, 2018. 3

[10] H. Huang, D. Li, Z. Zhang, X. Chen, and K. Huang. Adversarially occluded samples for person re-identification. In *Proceedings of the IEEE Conference on Computer Vision and Pattern Recognition*, pages 5098–5107, 2018. 1, 2

[11] T.-Y. Lin, P. Goyal, R. Girshick, K. He, and P. Dollár. Focal loss for dense object detection. In *Proceedings of the IEEE international conference on computer vision*, pages 2980–2988, 2017. 8

[12] T.-Y. Lin, M. Maire, S. Belongie, J. Hays, P. Perona, D. Ramanan, P. Dollár, and C. L. Zitnick. Microsoft coco: Common objects in context. In *European conference on computer vision*, pages 740–755. Springer, 2014. 5

[13] W. Liu, D. Anguelov, D. Erhan, C. Szegedy, S. Reed, C.-Y. Fu, and A. C. Berg. Ssd: Single shot multibox detector. In *Proceedings of the European conference on computer vision*, pages 21–37. Springer, 2016. 8

[14] J. Redmon and A. Farhadi. Yolo9000: better, faster, stronger. In *Proceedings of the IEEE conference on computer vision and pattern recognition*, pages 7263–7271, 2017. 8

[15] S. Ren, K. He, R. Girshick, and J. Sun. Faster r-cnn: Towards real-time object detection with region proposal networks. In *Advances in neural information processing systems*, pages 91–99, 2015. 6, 7, 8

[16] R. R. Selvaraju, M. Cogswell, A. Das, R. Vedantam, D. Parikh, and D. Batra. Grad-cam: Visual explanations from deep networks via gradient-based localization. In *Proceedings of the IEEE International Conference on Computer Vision*, pages 618–626, 2017. 3, 4

[17] A. Shrivastava, A. Gupta, and R. Girshick. Training region-based object detectors with online hard example mining. In *Proceedings of the IEEE Conference on Computer Vision and Pattern Recognition*, pages 761–769, 2016. 1

[18] K. K. Singh and Y. J. Lee. Hide-and-seek: Forcing a network to be meticulous for weakly-supervised object and action localization. In *Proceedings of the IEEE International Conference on Computer Vision*, pages 3544–3553, 2017. 3

[19] Y. Song, C. Ma, X. Wu, L. Gong, L. Bao, W. Zuo, C. Shen, R. W. Lau, and M.-H. Yang. Vital: Visual tracking via adversarial learning. In *Proceedings of the IEEE Conference on Computer Vision and Pattern Recognition*, pages 8990–8999, 2018. 3

[20] J. T. Springenberg, A. Dosovitskiy, T. Brox, and M. Riedmiller. Striving for simplicity: The all convolutional net. *arXiv preprint arXiv:1412.6806*, 2014. 3

[21] X. Wang, A. Shrivastava, and A. Gupta. A-fast-rcnn: Hard positive generation via adversary for object detection. In *Proceedings of the IEEE Conference on Computer Vision and Pattern Recognition*, pages 2606–2615, 2017. 1, 3, 5, 6, 7

[22] X. Wang, T. Xiao, Y. Jiang, S. Shao, J. Sun, and C. Shen. Repulsion loss: detecting pedestrians in a crowd. In *Proceedings of the IEEE Conference on Computer Vision and Pattern Recognition*, pages 7774–7783, 2018. 1, 2

[23] S. Woo, J. Park, J.-Y. Lee, and I. So Kweon. Cbam: Convolutional block attention module. In *Proceedings of the European Conference on Computer Vision*, pages 3–19, 2018. 3

[24] S. Zagoruyko and N. Komodakis. Paying more attention to attention: Improving the performance of convolutional neural networks via attention transfer. *arXiv preprint arXiv:1612.03928*, 2016. 3

[25] M. D. Zeiler and R. Fergus. Visualizing and understanding convolutional networks. In *Proceedings of the European conference on computer vision*, pages 818–833, 2014. 3

[26] S. Zhang, L. Wen, X. Bian, Z. Lei, and S. Z. Li. Occlusion-aware r-cnn: detecting pedestrians in a crowd. In *Proceedings of the European Conference on Computer Vision*, pages 637–653, 2018. 1, 2

[27] S. Zhang, J. Yang, and B. Schiele. Occluded pedestrian detection through guided attention in cnns. In *Proceedings of the IEEE Conference on Computer Vision and Pattern Recognition*, pages 6995–7003, 2018. 3

[28] Z. Zhong, L. Zheng, G. Kang, S. Li, and Y. Yang. Random erasing data augmentation. *arXiv preprint arXiv:1708.04896*, 2017. 2, 5

[29] B. Zhou, A. Khosla, A. Lapedriza, A. Oliva, and A. Torralba. Learning deep features for discriminative localization. In *Proceedings of the IEEE conference on computer vision and pattern recognition*, pages 2921–2929, 2016. 3

[30] C. Zhou and J. Yuan. Bi-box regression for pedestrian detection and occlusion estimation. In *Proceedings of the European Conference on Computer Vision*, pages 135–151, 2018. 2